AFRL-RX-WP-TP-2009-4083

THERMAL CONDUCTIVITY REDUCTION IN FULLERENE-ENRICHED *p*-TYPE BISMUTH TELLURIDE-BASED COMPOSITES (PREPRINT)

J.E. Spowart, N. Gothard, and Terry M. Tritt

Metals Branch
Metals, Ceramics and NDE Division

APRIL 2009

AIR FORCE RESEARCH LABORATORY
MATERIALS AND MANUFACTURING DIRECTORATE
WRIGHT-PATTERSON AIR FORCE BASE, OH 45433-7750
AIR FORCE MATERIEL COMMAND
UNITED STATES AIR FORCE

REPORT DOCUMENTATION PAGE

Form Approved
OMB No. 0704-0188

1. REPORT DATE *(DD-MM-YY)*	2. REPORT TYPE	3. DATES COVERED *(From - To)*
April 2009	Journal Article Preprint	01 April 2009 – 01 April 2009

4. TITLE AND SUBTITLE
THERMAL CONDUCTIVITY REDUCTION IN FULLERENE-ENRICHED *p*-TYPE BISMUTH TELLURIDE-BASED COMPOSITES (PREPRINT)

5a. CONTRACT NUMBER
In-house

5b. GRANT NUMBER

5c. PROGRAM ELEMENT NUMBER
62102F

6. AUTHOR(S)
J.E. Spowart (AFRL/RXLMD)
N. Gothard and Terry M. Tritt (Clemson University)

5d. PROJECT NUMBER
4347

5e. TASK NUMBER
RG

5f. WORK UNIT NUMBER
M02R4000

7. PERFORMING ORGANIZATION NAME(S) AND ADDRESS(ES)

Metals Branch (RXLMD)
Metals, Ceramics and NDE Division
Materials and Manufacturing Directorate
Wright-Patterson Air Force Base, OH 45433-7750
Air Force Materiel Command, United States Air Force

Department of Physics and Astronomy
Clemson University
Clemson, SC 29634

8. PERFORMING ORGANIZATION REPORT NUMBER
AFRL-RX-WP-TP-2009-4083

9. SPONSORING/MONITORING AGENCY NAME(S) AND ADDRESS(ES)
Air Force Research Laboratory
Materials and Manufacturing Directorate
Wright-Patterson Air Force Base, OH 45433-7750
Air Force Materiel Command
United States Air Force

10. SPONSORING/MONITORING AGENCY ACRONYM(S)
AFRL/RXLMD

11. SPONSORING/MONITORING AGENCY REPORT NUMBER(S)
AFRL-RX-WP-TP-2009-4083

12. DISTRIBUTION/AVAILABILITY STATEMENT
Approved for public release; distribution unlimited.

13. SUPPLEMENTARY NOTES
To be submitted to Physics Status Solidi (A)
PAO Case Number and clearance date: 88ABW-2009-1168, 25 March 2009.
The U.S. Government is joint author on this work and has the right to use, modify, reproduce, release, perform, display, or disclose the work.

14. ABSTRACT
We present a systematic study of the effects of fullerene nano-inclusions upon a *p*-type bismuth-antimony-telluride matrix, where the ultimate goal is maximizing the figure of merit by reducing the thermal conductivity. Nanocomposites consisting of a bismuth telluride matrix with fullerene inclusions have been prepared both by mechanical mixing and ball milling, with the final consolidation in each case achieved by uniaxial hot pressing. A series of samples was produced with fullerene concentrations ranging from fractional levels to several molar percent, and the effects of the fullerene additions upon the resulting microstructure have been considered. Thermal and electrical transport properties have been measured from 10 K to 300 K, and the data are discussed in light of the underlying physical mechanisms.

15. SUBJECT TERMS
fullerene nano-inclusions, bismuth-antimony-telluride matrix, uniaxial hot pressing

16. SECURITY CLASSIFICATION OF:			17. LIMITATION OF ABSTRACT:	18. NUMBER OF PAGES	19a. NAME OF RESPONSIBLE PERSON (Monitor)
a. REPORT	b. ABSTRACT	c. THIS PAGE			Jonathan Spowart
Unclassified	Unclassified	Unclassified	SAR	28	19b. TELEPHONE NUMBER *(Include Area Code)* N/A

Standard Form 298 (Rev. 8-98)
Prescribed by ANSI Std. Z39-18

Thermal conductivity reduction in fullerene-enriched *p*-type bismuth telluride-based composites

N. Gothard[1], J.E. Spowart[2], and Terry M. Tritt[1*]

[1]Department of Physics and Astronomy, Clemson University, Clemson, SC 29634

[2]Air Force Research Laboratory, Materials and Manufacturing Directorate, WPAFB, OH 45433

ABSTRACT

We present a systematic study of the effects of fullerene nano-inclusions upon a *p*-type bismuth-antimony-telluride matrix, where the ultimate goal is maximizing the figure of merit by reducing the thermal conductivity. Nanocomposites consisting of a bismuth telluride matrix with fullerene inclusions have been prepared both by mechanical mixing and ball milling, with the final consolidation in each case achieved by uniaxial hot pressing. A series of samples was produced with fullerene concentrations ranging from fractional levels to several molar percent, and the effects of the fullerene additions upon the resulting microstructure have been considered. Thermal and electrical transport properties have been measured from 10 K to 300 K, and the data are discussed in light of the underlying physical mechanisms.

* Corresponding author: ttritt@clemson.edu

INTRODUCTION

The efficiency of thermoelectric heat-power conversion is directly related to the dimensionless figure of merit, or "ZT", of a material, where $ZT \equiv \alpha^2 \sigma T / (\kappa_e + \kappa_L)$. Here α is the thermopower, σ is the electrical conductivity, T is the temperature, and κ_e and κ_L are the charge carrier and lattice thermal conductivities, respectively. Thermoelectric materials research typically focuses first on maximizing the power factor (defined as $\alpha^2 \sigma T$) via elemental substitution, followed by attempts to reduce the thermal conductivity by the introduction of phonon scattering mechanisms [1]. In the case of many bulk materials, however, a plateau of performance in the power factor has already been achieved, with many of the best candidates for high ZT being near-fully optimized at ZT values below those needed for widespread industrial implementation (i.e. ZT = 2-3 [2]).

Recently, it has been suggested that low dimensional morphologies may provide additional avenues for ZT enhancement, with nanostructured thermoelectric materials benefitting either from power factor enhancement due to quantum confinement effects [3] or from a reduction in thermal conductivity via phonon boundary scattering due to the large number of interfaces [4]. To date, a number of experimental studies have demonstrated reduction of thermal conductivity in nanostructured materials [5,6,7], and some results have indicated that the electronic properties can also be enhanced by the presence of nanoscale grains or nanoscale regions (nanodots) in the material [7,8].

In spite of these exciting advances, the issue remains whether such principles can be implemented with ease and repeatability on the bulk scale. To address this scaling

problem, the concept of a nanocomposite consisting of a bulk matrix + nanomaterials has been pursued [9,10], where the bulk matrix is chosen from a near-optimized thermoelectric material such as PbTe [11], $CoSb_3$ [12], or bismuth telluride [13]. A recent study, moreover, has shown that ball milling of bismuth telluride matrix powders in an inert atmosphere is effective in increasing the figure of merit in the bismuth telluride system in due to the presence of naturally occurring nanoparticle inclusions [7]. Another study incorporated hydrothermally grown [14] bismuth telluride particles into a bismuth telluride matrix, with the result that the degree of boundary scattering of both phonons and electrons increased, but the decrease in the electrical conductivity dominated potential benefits to the figure of merit [13]. Arguably, the similarity of the matrix ($Bi_2(Te,Se)_3$) and the nanoparticles (Bi_2Te_3, 30 nm) in both size and composition may somewhat have masked the effects of the nanoparticles upon the composite, precluding an adequate quantification of their effects. To address this problem, it is of interest to investigate the effects of nanoparticles that have significantly different compositions, elastic properties, and sizes than those of the matrix particles. In the work presented herein, C_{60} (~0.7 nm diameter) was selected as a readily available nanomaterial in this regard, considering previous work in the Si-Ge [15,16] and $CoSb_3$ [17] systems, where C_{60} was found to be an effective candidate for reducing the thermal conductivity by either small or large defect scattering. It is shown herein that either large defect or phonon boundary scattering can be employed to reduce the thermal conductivity of the resultant nanocomposites, and that the type of scattering is determined by the geometry of the nanoparticle inclusions, which is in turn determined by the preparation technique.

METHOD

The composites used in this study were prepared using a matrix obtained from a commercial *p*-type $(Bi,Sb)_2Te_3$ ingot obtained from Marlow Industries, into which C_{60} was incorporated at various molar percentages. Two preparation techniques were used: ball milling and mechanical dry-mixing, and the nanocomposite samples will hereafter be referred to on the basis of the processing route ("ball milled" or "mixed"). For preparation by ball milling, the ingot was first coarsely ground by mortar and pestle, and then the matrix powders were loaded together with C_{60} into a ball mill, where mixing along with further grinding of the matrix powders was accomplished. In an attempt to minimize oxidation and surface contamination, the ball mill was placed within a glove box. In the case of 3-axis mixing, the ingot was ground by mortar and pestle and the powders were then sieved, after which powders of approximate size distribution 5-15 μm were mixed together with C_{60} in a Turbula® 3-axis mixer. The sieves were employed in an attempt to control the size distribution of the matrix phase, the goal being a near-uniform, micron-sized matrix. The final step in consolidation in either case was uniaxial hot pressing at 300-350°C in an argon atmosphere, resulting in a mechanically robust cylindrical pellet having dimensions of approximately 12 mm diameter and 2 mm thickness. X-ray diffraction and Raman spectroscopy were used to verify that C_{60} had survived the processing intact, and that there were no detectable additional carbon phases.

Thermopower and electrical resistivity were measured from 10 K to room temperature on samples measuring roughly 2mm x 2mm x 8mm by a 4-probe, fast-switching DC configuration in a custom-designed system [18]. Thermal conductivity data were acquired

on the same samples from 25 K to 300 K using a custom-built steady-state measurement system [19]. Measurements of the Hall Effect were performed on a Quantum Design® Physical Properties Measurement System (PPMS), and from this the carrier concentration and electronic mobility were calculated. To promote accuracy and reproducibility in the measurements, multiple samples were cut from each pellet and in most cases multiple pellets were pressed with identical nominal percentages of C_{60}.

DATA

Microstructure

Characterization by SEM was performed on an FEI Quanta® FESEM. The microstructural differences caused by the different processing techniques as well as by the addition of C_{60} are shown in Figure 1. The microstructure for the 0% reference sample prepared by mixing reveals an average grain size in the range of 5-15 μm, consistent with what was observed in the Bi_2Te_3 / $Bi_2(Te,Se)_3$ nanocomposites [13], and there is also a moderate degree of porosity combined with minor elemental inhomogeneity. The introduction of C_{60} into the composite results in large carbon aggregations, even at small percentages (figure 1b), but the aggregations can extend for hundreds of microns as the nominal percentage of C_{60} is increased (figure 1b inset). These aggregations were verified by EDX to be regions of high carbon concentration, with little or no carbon being found in other areas of the sample.

When ball milling is used for grinding and mixing, the effects upon the microstructure are a decrease in the average grain size, and there appears also to be a slight increase in the

degree of elemental inhomogeneity (figure 1c). Here, the largest grains are on the order of 5 μm, but large areas of sub-micron-sized grains are also apparent. Figures 1d and 1d (inset) show the effect of adding C_{60} to the composites in 1 and 5 molar percent, respectively. In such cases, the degree of carbon dispersion between the matrix grains is greatly increased, and the largest matrix grains are easily identifiable as isolated anisotropic fragments with widths on the order of 1-3 μm, and lengths no longer than 5-8 μm. Figure 2a shows another cross section from a 5% ball milled sample, with figures 2b and 2c showing elemental maps of the presence of Sb and C, respectively, where Sb is taken as representative of the matrix (composition $Bi_{0.4}Sb_{1.6}Te_3$). It should be noted also that some isolated Bi-rich regions have been found, and that difficulties have been encountered in resolving the Te signal, which is poor due to the difficulty of obtaining a strong signal-to-noise ratio as a result of an overlap with the Sb peak. Nevertheless, the dispersion of carbon between the matrix grains is clearly visible in figure 2c.

Transport

Figure 3 shows the lattice thermal conductivity (TC) data for the two series of composites as well as the ingot as a function of a) temperature and b) percentage C_{60}, with only a select number of data curves presented in figure 3a for the sake of legibility. The lattice TC data presented here have not been corrected for any possible radiation effects. As such effects are generally expected to become of significance only above 200 K, figure 3b shows the data values at 200 K. Figure 3a shows that the low temperature thermal conductivity peak is significantly suppressed both as a function of nanoparticle percentage as well as of ball milling, implying that both the introduction of nanoparticles as well as

processing by ball milling have served to increase dramatically the degree of boundary scattering of phonons. Accordingly, this effect is quite pronounced in the ball milled samples that contain C_{60}. Figure 3b indicates that the most important effect upon the thermal conductivity in the near-room temperature range is the addition of fullerenes, but that this effect does not become especially pronounced until after approximately 1 molar % C_{60}.

Figure 4 shows the response of several room temperature thermoelectric properties values to the addition of C_{60}. The behavior of the power factor mirrors that of the electrical resistivity, decreasing just as the resistivity increases. It is clear that these effects are due primarily to significant C_{60} incorporation, but that processing by ball-milling also plays an important role. While there is a slight decrease in thermopower as C_{60} is added, the figure of merit data predominantly reflects the increase in the resistivity, which counteracts the reduced thermal conductivity values of many of the samples.

DISCUSSION

A comparison of the changes in electrical resistivity and percentage of theoretical density shows that the resistivity trends cannot be attributed simply to porosity or poor densification, as the densities are generally high and do not correlate with increases in the resistivity (table 1). In fact, the high densities of the ball milled samples that contain some fraction of C_{60} suggest that the finer dispersion of C_{60} in these samples may be helping to fill pores in the microstructure. As seen in figure 3a, it was noted that the primary effects of the processing as well as of the nanoparticles upon the thermal conductivities of the

composites occur at low temperatures, due to scattering of phonons by the grain boundaries. If grain boundary scattering of charge carriers is also the primary source of reduced electrical conductivity in the low temperature region, one would expect $\ln(\mu T^{1/2})$ to be proportional to 1/kT [20], and this is shown to hold true at low (but not high) temperatures in figure 5. Further analysis is therefore needed to understand the reason for the room temperature increases in resistivity shown in figure 4. Table 2 demonstrates the effects of mixing vs. ball milling upon the charge carrier mobility and carrier concentration, as compared to the electrical resistivity. The reference samples prepared both by mixing as well as by ball milling have mobility values that are quite similar (345 and 327 $cm^2V^{-1}s^{-1}$ respectively). When C_{60} is added by ball milling, the mobility decreases, but when it is added by mixing, the mobility increases, an effect that runs contrary to expectation. Further, these effects are mirrored by the slight changes in carrier concentration that accompany C_{60} incorporation—i.e. *n* increases mildly in the ball milled samples but decreases in the mixed samples as C_{60} is added. In general, C_{60} is expected to act as an electron acceptor [21]. The fact that ball milling causes the carrier concentration to increase as a function of C_{60}, therefore, could indicate that the increased degree of homogenization is helping seed the composite with additional holes, as the bismuth telluride-C_{60} contact area is considerably greater in these samples. As the resistivity is expected to follow the relationship $\rho = 1/ne\mu$, it follows that the ball milled samples, which have higher carrier concentrations, should have lower resistivities, but the impact of the nanoparticles upon the mobility, which decreases in these samples, is the deciding factor from a standpoint of the quantity $1/n\mu$. The correlation of the experimentally measured resistivity with this quantity is not 100%, however, and this is likely attributable

to sample inhomogeneity as well as the potential for mild oxidation to occur during the various steps of processing.

Regarding phonon transport, as the temperature nears 300 K, the mean free path of the phonon, l_{ph}, is estimated to be on the order of 0.30 nm, using the result from kinetic theory: $\kappa_L = \frac{1}{3} C_v v l_{ph}$, where $C_v = 1.24\text{x}10^6 J \cdot K^{-1} m^{-3}$ and $v = 3\text{x}10^3 \, m/s$ for bismuth telluride [22]. For the large aggregations produced by 3-axis mixing, which have cross sections of tens to hundreds of microns, phonon scattering by large defects is therefore expected. When ball milling is used, however, the fine dispersion of the fullerene molecules suggests that boundary scattering by fullerenes that have filled the gaps between the matrix particles is the dominant effect, in accordance with the lattice thermal conductivity data. This is consistent with the low temperature dependence of the lattice thermal conductivity, where the ball milled samples show substantially greater TC reduction, which reflects a greater degree of boundary scattering than the mixed samples (figure 3a).

Figure 6 shows the radiation-corrected total thermal conductivity data for the results presented herein, as well as previously unpublished data using ball milling to form a Bi_2Te_3 nanoparticle / $Bi_2(Te,Se)_3$ matrix. The effects of ball milling are again noticeable, as all ball-milled samples exhibit decreased TC values at low temperatures in comparison to their counterparts prepared by mixing. Interestingly, the Bi_2Te_3 / $Bi_2(Te,Se)_3$ composite matches the TC value of approximately 1.1 W/m-K, as reported in reference [7], most closely, while the 0% ball milled reference sample, which is expected to be more compositionally similar to those composites, gives an increased TC value. Such

differences may be attributed to variations in the preparation techniques or to the fact that the Bi_2Te_3 / $Bi_2(Te,Se)_3$ composites are the only ones that use an *n*-type bismuth-telluride-selenium matrix. Additional room temperature thermal conductivity reduction can be achieved, however, by introducing C_{60} particles, regardless of the preparation technique, with the thermal conductivity reduction becoming especially pronounced when ball milling is used to improve the C_{60} dispersion. The net result is that C_{60} incorporation leads to room temperature thermal conductivity values that are approximately 0.15 W/m-K less than the near-room-temperature value reported in reference [7] when prepared by mixing and approximately 0.25 W/m-K less when prepared by ball milling. Moreover, the ball milled C_{60} / $(Bi,Sb)_2Te_3$ nanocomposite shows a significant reduction in thermal conductivity across the entire temperature range, but especially at low temperatures, where the longer wavelength phonons are particularly susceptible to boundary scattering effects. At higher temperatures, where the phonon wavelengths are shorter, geometrical scattering by large defects is more prominent [23], which helps explain why thermal conductivity reduction occurs primarily near room temperature in the samples with large aggregates of C_{60} (mixed).

CONCLUSIONS

C_{60} incorporation by either 3-axis mixing or ball milling has been found useful for lowering the thermal conductivity in bismuth telluride-based composites. Preparation by 3-axis mixing yields large aggregates of fullerenes whereas ball milling results in a more uniform dispersion of C_{60} between the matrix grains, which are generally smaller in size as a result of ball milling. Considering the size of the C_{60} aggregates in relation to the phonon

mean free path indicates that the choice of the preparation technique can lead to either large defect or boundary scattering of phonons. Further, introduction of the fine-grained fullerene particles results in room temperature thermal conductivity values that are decreased beyond those obtained either by incorporating bismuth telluride nanoparticles into the matrix or by ball milling the matrix in the absence of nanoparticles. Such a reduction occurs regardless of the preparation technique, although a more significant reduction in thermal conductivity throughout the low-to-intermediate temperature range is achieved if the C_{60} dispersion is increased by ball milling. The primary effect of the fullerenes, then, appears to be an increase in the degree both of phonon and charge carrier grain boundary scattering, as well as an increase in room temperature electrical resistivity that effectively offsets the benefits of decreasing the thermal conductivity, from a standpoint of the figure of merit. The interplay of carrier concentration and mobility leaves room , however,for additional work that could result in further optimization of these materials.

ACKNOWLEDGEMENTS

The authors acknowledge support from Air Force Research Laboratory, Materials and Manufacturing Directorate, through a Collaborative Research and Development contract with Universal Technologies Corporation (UTC-Air Force/0978-205-2006541). Special thanks to Dr. Jeff Sharp of Marlow Industries for supplying the *n*- and *p*-type bismuth telluride ingots. We also acknowledge Dr. Christopher A. Crouse for his valuable help with FESEM analysis as well as Dr. Jian He and Dr. Bevan E. Elliot for helpful discussions.

REFERENCES

[1] *New Materials and Performance Limits for Thermoelectric Cooling*, in CRC Handbook on Thermoelectrics , edited by D.M. Rowe (CRC Press, Boca Raton, 1995), pp. 407-440.

[2] J. Yang and T. Caillat, MRS Bulletin **31**, 224 (2006).

[3] L.D. Hicks and M.S. Dresselhaus, Phys. Rev. B **47**, 12727 (1993).

[4] J.W. Sharp, S.J. Poon, and H.J. Goldsmid, Phys. Stat. Sol. (a) **187**, 507 (2001).

[5] R. Venkatasubramanian, E. Siivola, T. Colpitts, B. O'Quinn, Nature **413**, 597 (2001).

[6] T.C. Harman, P.J. Taylor, M.P. Walsh, B.E. LaForge, Science **297**, 2229 (2002).

[7] B. Poudel, Q. Hao, Y. Ma, Y. Lan, A. Minnich, B. Yu, X. Yan, D. Wang, A. Muto, D. Vashaee, X. Chen, J. Liu, M.S. Dresselhaus, G. Chen, and Z. Ren, Science **320**, 634 (2008).

[8] K.F. Hsu, S. Loo, F. Guo, W. Chen, J.S. Dyck, C. Uher, T. Hogan, E.K. Polychroniadis, M.G. Kanatzidis, Science **303**, 818 (2004).

[9] M.S. Dresselhaus, G. Chen, M.Y. Tang, R.G. Yang, H. Lee, D.Z. Wang, Z.F. Ren, J.P. Fleurial, and P. Gogna, Mater. Res. Soc. Symp. Proc. **886**, 170056 (2005).

[10] T.M. Tritt, B. Zhang, N. Gothard, J. He, X. Ji, D. Thompson, and J.W. Kolis, Mater. Res. Soc. Symp. Proc. **886**, 170104 (2005).

[11] J. Martin, G.S. Nolas, W. Zhang, and L. Chen, Appl. Phys. Lett. **90**, 222122 (2007).

[12] P.N. Alboni, X.Ji, J. He, N. Gothard, and T.M. Tritt, J. Appl. Phys. **103**, 113707 (2008).

[13] N. Gothard, X. Ji, J. He, and T.M. Tritt, J. Appl. Phys. **103**, 054314 (2008).

[14] X.B. Zhao, X.H. Ji, Y.H. Yang, G.S. Cao, and J.P. Tu, Appl. Phys. A: Mater. Sci. Process. **80**, 1567 (2005).

[15] B.A. Cook, J.L. Harringa, S. Loughin, Mat. Sci. Eng. **B41**, 280 (1996).

[16] G.A. Slack and M. Hussain, J. Appl. Phys. **70**, 2694 (1991).

[17] X. Shi, L. Chen, J. Yang, G.P. Meisner, Appl. Phys. Lett. **84**, 2301 (2004).

[18] A.L. Pope, R.T. Littleton IV, and T.M. Tritt, Rev. Sci. Instr. **72**, 3129 (2001).

[19] A.L. Pope, B. Zawilski, and T.M. Tritt, Cryogenics **41**, 725 (2001).

[20] J.W. Orton and M.J. Powell, Rep. Prog. Phys. **43**, 1263 (1980).

[21] Q. Xie, E. Perez-Cordero, and L. Echegoyen, J. Am. Chem. Soc. **114**, 3978 (1992).

[22] H.H. Landolt and R. Börnstein, *Numerical Data and Functional Relationships in Science and Technology*, New Series, vol. 17f (Springer-Verlag, Berlin, 1983), pp. 272-278.

[23] J.W. Vandersande, Phys. Rev. B **15**, 2355 (1977).

Figure Captions

Fig. 1 FESEM images in backscattering mode for a) 0% mixed reference sample, b) 1% C_{60} (mixed) with 5% C_{60} (mixed) in the inset, c) 0% ball milled reference, d) 1% C_{60} (ball milled) with 5% C_{60} (ball milled) in the inset.

Fig. 2 a) Backscattering image of 5% C_{60} (ball milled), b) Sb elemental map of cross section depicted in a), and c) C elemental map of the same, showing carbon aggregations between grains of bismuth-antimony-telluride composition.

Fig. 3 a) Lattice thermal conductivity vs. temperature for the C_{60} samples (mixed and ball milled), showing a significant reduction in the low temperature peak. b) Lattice TC data at 200 K.

Fig. 4 Room temperature values for the mixed and ball milled C_{60} / $(Bi,Sb_2)Te_3$ composites, showing a) resistivity, b) thermopower, c) power factor, and d) figure of merit as functions of C_{60} percentage.

Fig. 5 $\ln(\mu T^{1/2})$ vs. 1/kT for the mixed and ball milled C_{60} composites. The linearity in the low temperature range indicates charge carrier boundary scattering to be an important effect.

Fig. 6 Total thermal conductivity for select data, showing agreement with the results of Poudel, *et al.* [7], as well as room temperature TC reduction for both types of C_{60} / $(Bi,Sb)_2Te_3$composites. Also shown is data from a previously synthesized Bi_2Te_3 / $Bi_2(Te,Se)_3$ sample, where the Bi_2Te_3 nanoparticles were grown via a hydrothermal method.

Figure 1. FESEM backscattering images

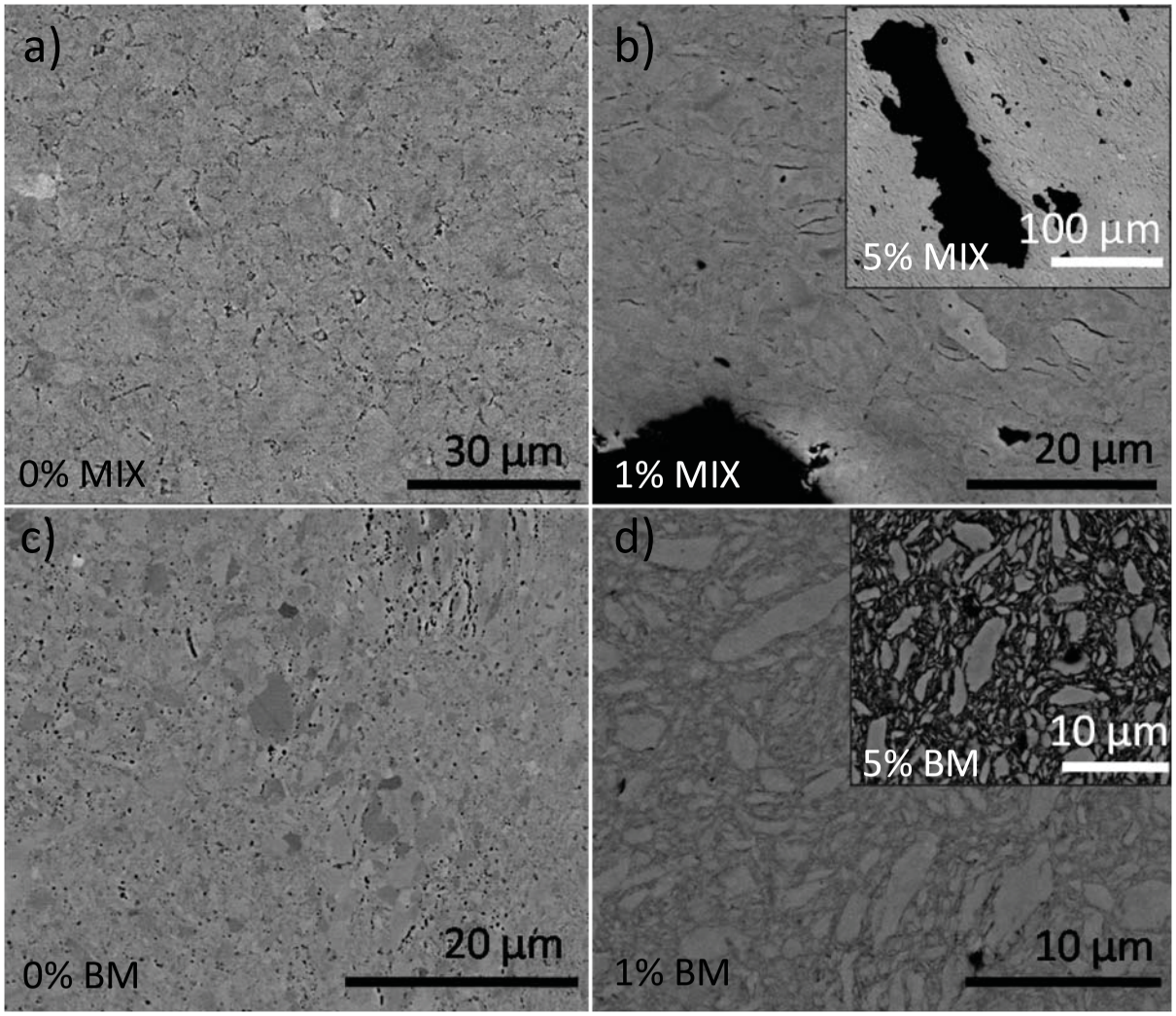

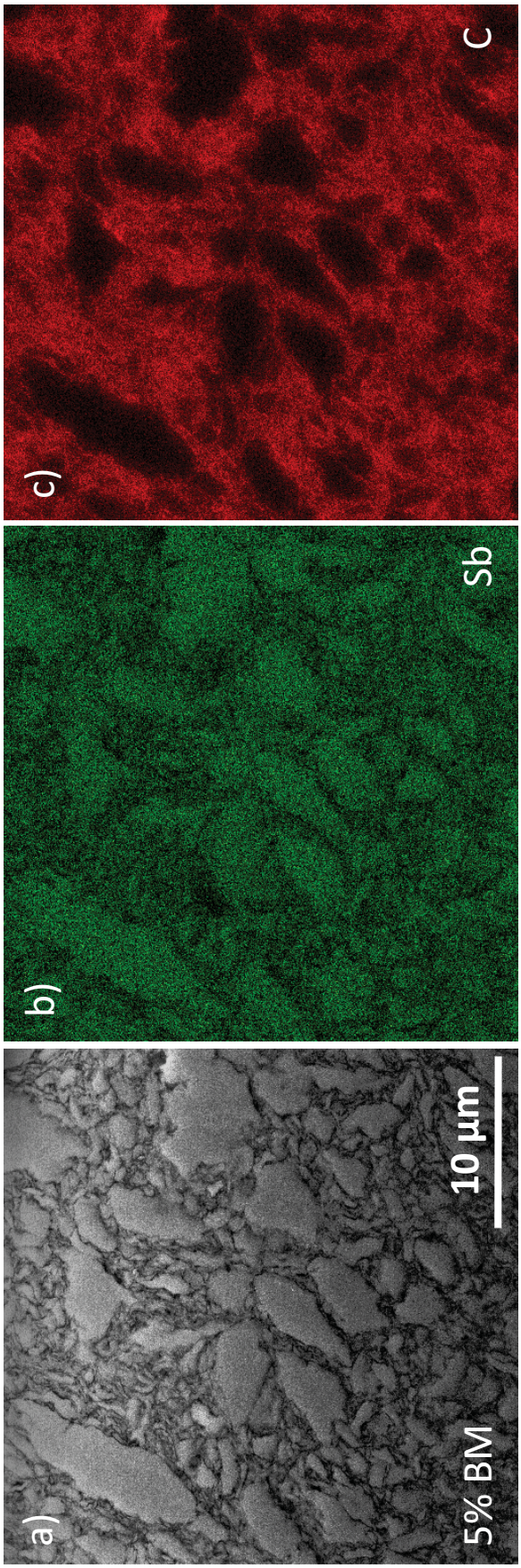

Figure 2

Figure 3

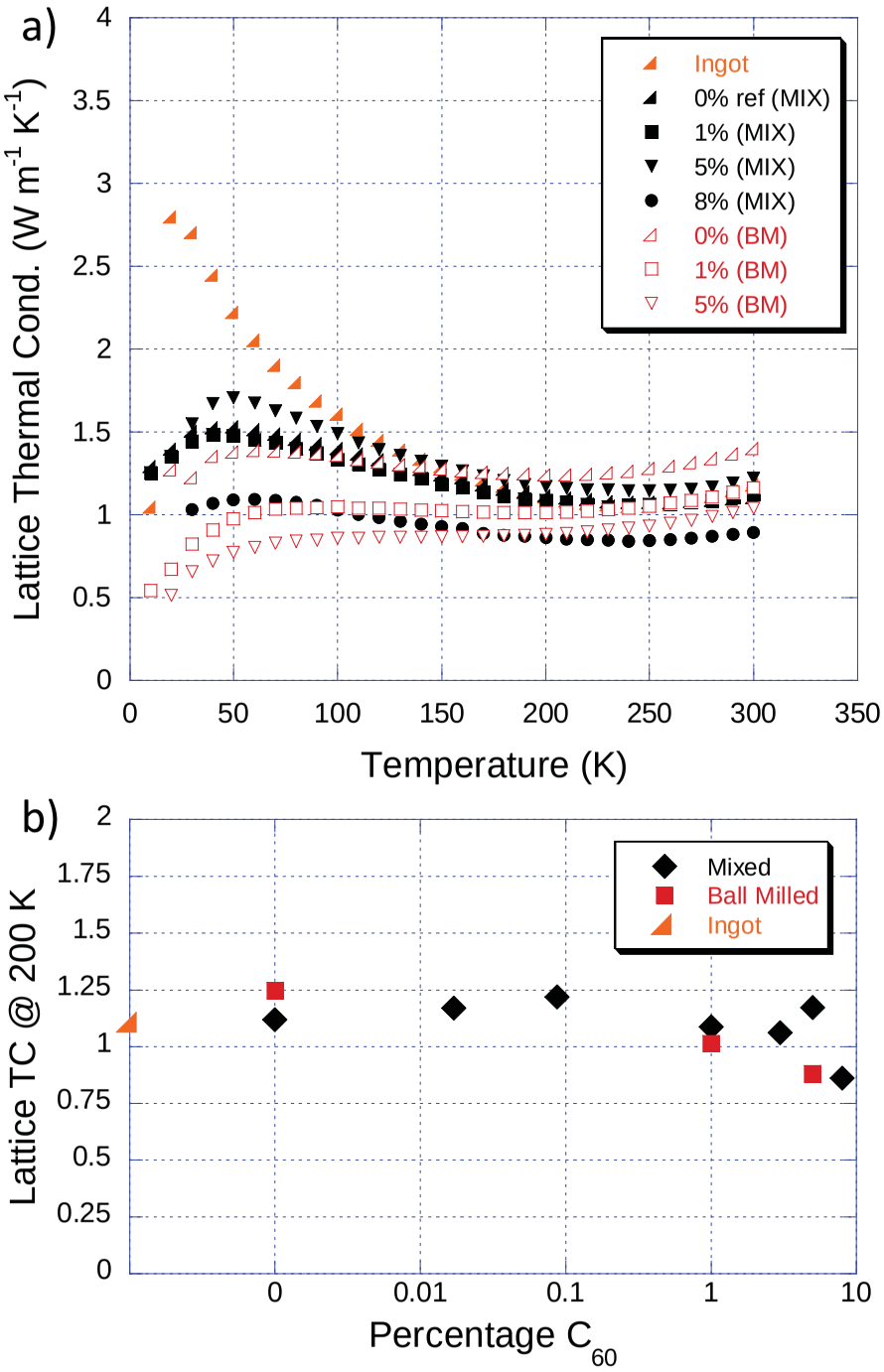
a)
Lattice Thermal Cond. (W m-1 K-1)
Temperature (K)
Ingot
0% ref (MIX)
1% (MIX)
5% (MIX)
8% (MIX)
0% (BM)
1% (BM)
5% (BM)
b)
Lattice TC @ 200 K
Percentage C60
Mixed
Ball Milled
Ingot

Figure 4

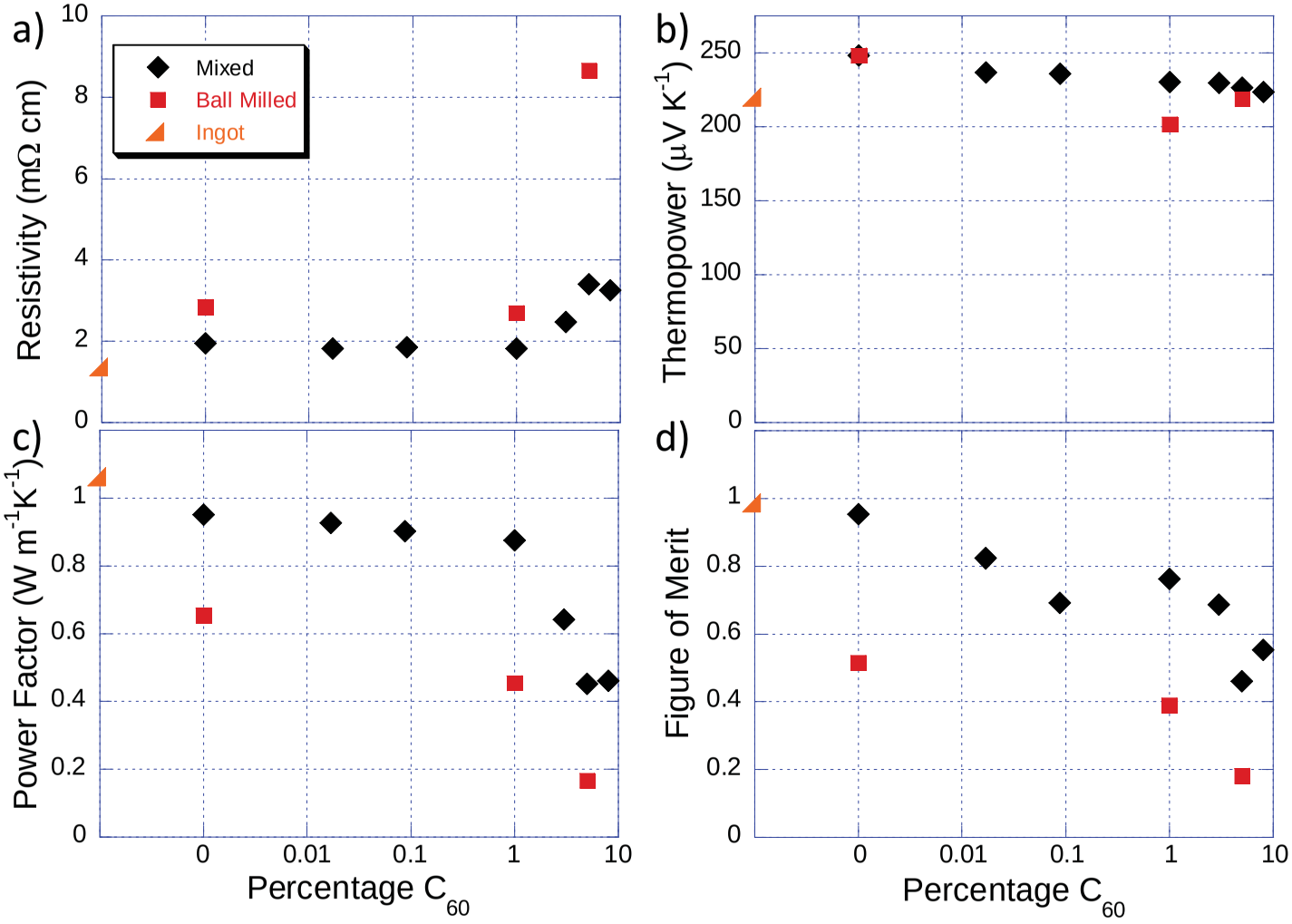
a)
b)
c)
d)
Mixed
Ball Milled
Ingot
Resistivity (mΩ cm)
Thermopower (μV K-1)
Power Factor (W m-1K-1)
Figure of Merit
Percentage C60
Percentage C60
0
0.01
0.1
1
10

Pct. C_{60} (MIX)	ρ (mΩ-cm)	density (% theo.)
0.00	1.95	97.8
0.02	1.82	92.3
0.09	1.85	100
1.00	1.82	86.8
3.00	2.48	100
5.00	3.41	97.3
8.00	3.25	94.1
Pct. C_{60} (BM)		
0.00	2.83	82.1
1.00	2.68	99.1
5.00	8.65	99.2

Table 1

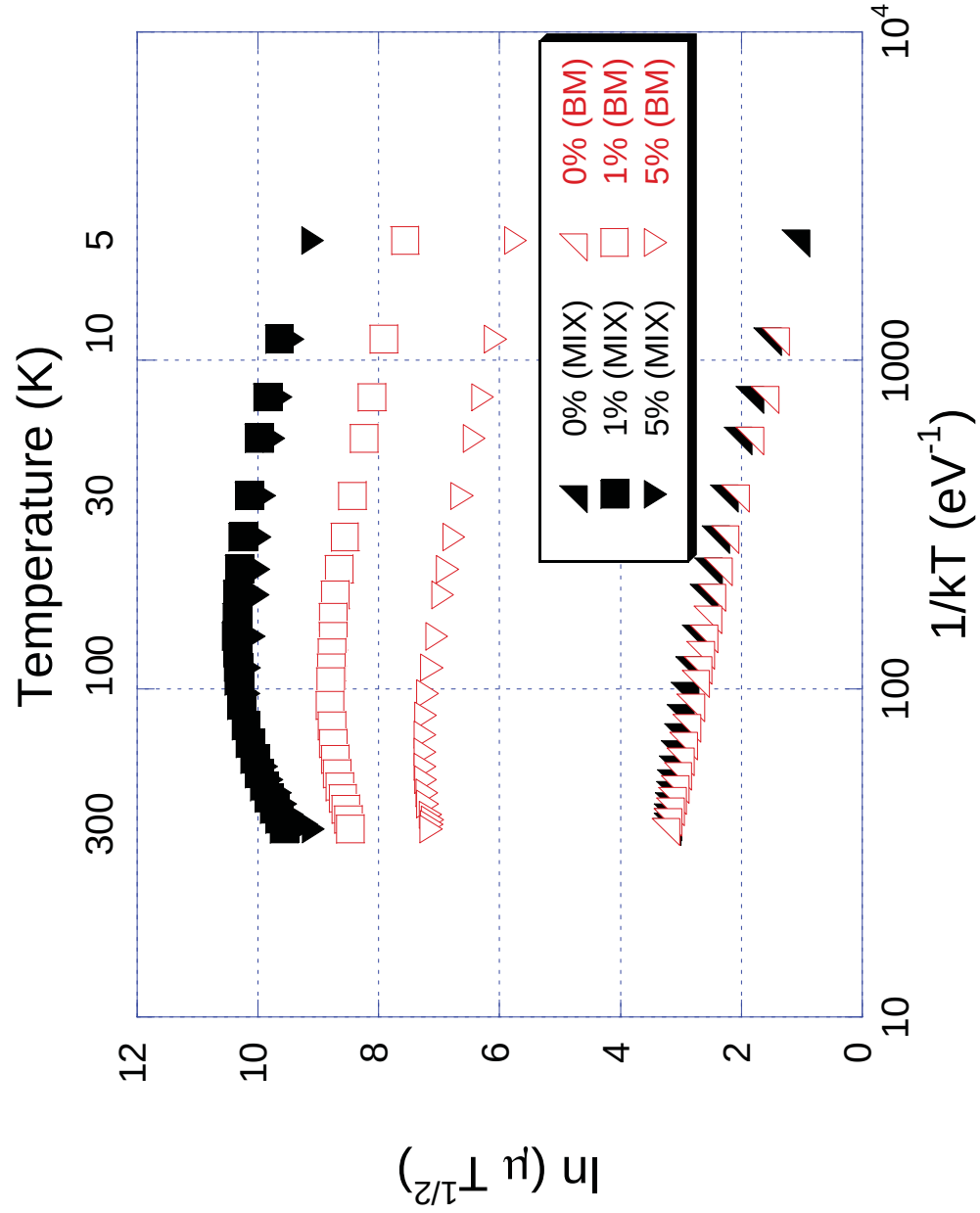
Temperature (K)
300
100
30
10
5
1/kT (eV-1)
10
100
1000
10^4
ln (μ T^1/2)
0
2
4
6
8
10
12
0% (MIX)
1% (MIX)
5% (MIX)
0% (BM)
1% (BM)
5% (BM)

Figure 5

Pct. C_{60} (MIX)	μ ($cm^2 V^{-1}s^{-1}$)	n ($10^{18} cm^{-3}$)	1/nμ (10^{-22} cm V s)	ρ (mΩ cm)
0.00	345.3	8.87	3.26	1.95
1.00	810.1	6.38	1.93	1.82
5.00	446.1	6.89	3.21	3.41
Pct. C_{60} (BM)				
0.00	327.4	6.67	4.58	2.83
1.00	272.4	10.98	3.34	2.68
5.00	71.2	10.13	13.9	8.65

Table 2

Figure 6

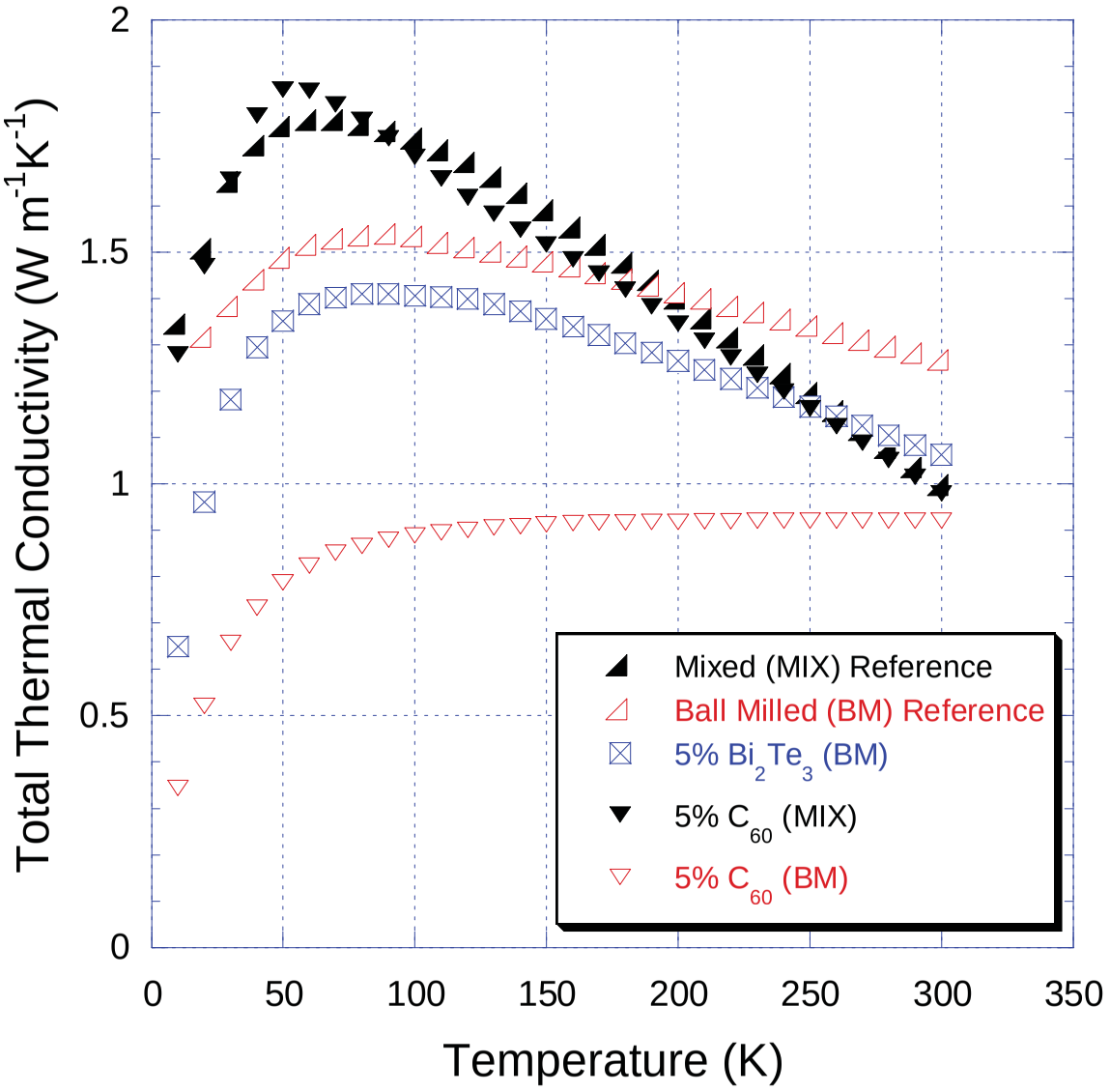
Total Thermal Conductivity (W m-1K-1)
Temperature (K)
0
0.5
1
1.5
2
0
50
100
150
200
250
300
350
Mixed (MIX) Reference
Ball Milled (BM) Reference
5% Bi2Te3 (BM)
5% C60 (MIX)
5% C60 (BM)